

# Flexible Glass Hybridized Colloidal Quantum Dots for Gb/s Visible Light Communications

**Foucher, C, Sufyan, MI, Guilhabert, BJE, Videv, S, Rajbhandari, S, Diaz, AG, Chun, H, Vithanage, DA, Turnbull, GA, Samuel, IDW, Faulkner, G, O'Brien, DC, Haas, H, Laurand, N & Dawson, MD**

**Author post-print (accepted) deposited by Coventry University's Repository**

**Original citation & hyperlink:**

Foucher, C, Sufyan, MI, Guilhabert, BJE, Videv, S, Rajbhandari, S, Diaz, AG, Chun, H, Vithanage, DA, Turnbull, GA, Samuel, IDW, Faulkner, G, O'Brien, DC, Haas, H, Laurand, N & Dawson, MD 2018, 'Flexible Glass Hybridized Colloidal Quantum Dots for Gb/s Visible Light Communications' *IEEE Photonics Journal*, vol 10, no. 1, 2200211 <https://dx.doi.org/10.1109/JPHOT.2018.2792700>

DOI 10.1109/JPHOT.2018.2792700

ISSN 1943-0655

ESSN 1943-0655

Publisher: IEEE

**© 20xx IEEE. Personal use of this material is permitted. Permission from IEEE must be obtained for all other uses, in any current or future media, including reprinting/republishing this material for advertising or promotional purposes, creating new collective works, for resale or redistribution to servers or lists, or reuse of any copyrighted component of this work in other works.**

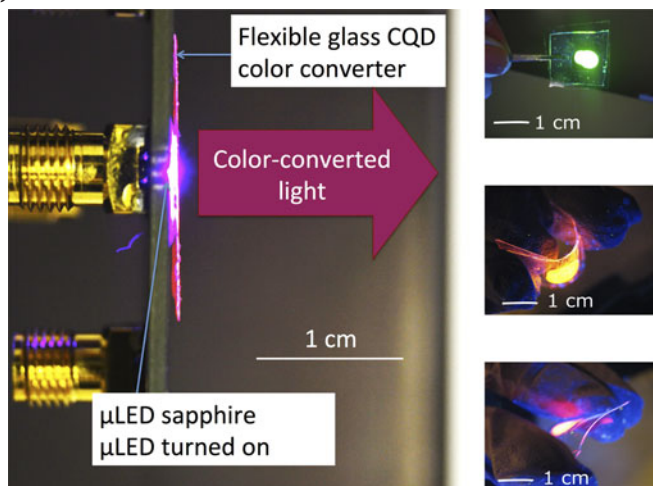
**Copyright © and Moral Rights are retained by the author(s) and/ or other copyright owners. A copy can be downloaded for personal non-commercial research or study, without prior permission or charge. This item cannot be reproduced or quoted extensively from without first obtaining permission in writing from the copyright holder(s). The content must not be changed in any way or sold commercially in any format or medium without the formal permission of the copyright holders.**

**This document is the author's post-print version, incorporating any revisions agreed during the peer-review process. Some differences between the published version and this version may remain and you are advised to consult the published version if you wish to cite from it.**

# Flexible Glass Hybridized Colloidal Quantum Dots for Gb/s Visible Light Communications

Volume 10, Number 1, February 2018

Caroline Foucher  
Mohamed Islim Sufyan, *Student Member, IEEE*  
Benoit Jack Eloi Guilhabert  
Stefan Videv  
Sujan Rajbhandari, *Member, IEEE*  
Ariel Gomez Diaz  
Hyunchae Chun  
Dimali A. Vithanage  
Graham A. Turnbull, *Senior Member, IEEE*  
Ifor D. W. Samuel  
Grahame Faulkner  
Dominic C. O'Brien  
Harald Haas  
Nicolas Laurand, *Member, IEEE*  
Martin D. Dawson, *Fellow, IEEE*



DOI: 10.1109/JPHOT.2018.2792700

1943-0655 © 2018 CCBY

# Flexible Glass Hybridized Colloidal Quantum Dots for Gb/s Visible Light Communications

Caroline Foucher,<sup>1</sup>  
Mohamed Islim Sufyan<sup>1b</sup>,<sup>2</sup> *Student Member, IEEE*,  
Benoit Jack Eloi Guilhabert<sup>1b</sup>,<sup>1</sup> Stefan Videv,<sup>2</sup>  
Sujan Rajbhandari<sup>1b</sup>,<sup>3\*</sup> *Member, IEEE*, Ariel Gomez Diaz<sup>1b</sup>,<sup>3</sup>  
Hyunchae Chun<sup>1b</sup>,<sup>3</sup> Dimali A. Vithanage,<sup>4</sup>  
Graham A. Turnbull<sup>1b</sup>,<sup>4</sup> *Senior Member, IEEE*, Ifor D. W. Samuel,<sup>4</sup>  
Grahame Faulkner,<sup>3</sup> Dominic C. O'Brien,<sup>3</sup> Harald Haas<sup>1b</sup>,<sup>2</sup>  
Nicolas Laurand<sup>1b</sup>,<sup>1</sup> *Member, IEEE*,  
and Martin D. Dawson<sup>1b</sup>,<sup>1</sup> *Fellow, IEEE*

<sup>1</sup>Institute of Photonics, Department of Physics, SUPA, University of Strathclyde, Glasgow G1 1RD, U.K.

<sup>2</sup>LiFi Research and Development Centre, Institute for Digital Communications, University of Edinburgh, Edinburgh EH9 3JL, U.K.

<sup>3</sup>Oxford Communications Research Group, Department of Engineering Science, University of Oxford, Oxford OX1 3PJ, U.K.

<sup>4</sup>Organic Semiconductor Centre, SUPA, School of Physics and Astronomy, University of St Andrews, St Andrews KY16 9SS, U.K.

DOI:10.1109/JPHOT.2018.2792700

This work is licensed under a Creative Commons Attribution 3.0 License. For more information, see <http://creativecommons.org/licenses/by/3.0/>

Manuscript received December 20, 2017; revised January 8, 2018; accepted January 9, 2018. Date of publication January 12, 2018; date of current version February 21, 2018. This work was supported by the EPSRC through the Program grant 'Ultra-parallel visible light communications (UP-VLC)' (EP/K00042X/1). Corresponding author: Nicolas Laurand (email: nicolas.laurand@strath.ac.uk).

\*S. Rajbhandari is now with the Centre for Mobility & Transport, School of Computing, Engineering and Mathematics, Coventry University, Coventry CV1 5FB, U.K.

**Abstract:** Color converting films of colloidal quantum dots (CQDs) encapsulated with flexible glass are integrated with microsize GaN LEDs ( $\mu$ LEDs) in order to form optical sources for high-speed visible light communications (VLC). VLC is an emerging technology that uses white and/or colored light from LEDs to combine illumination and display functions with the transmission of data. The flexible glass/CQD format addresses the issue of limited modulation speed of typical phosphor-converted LEDs while enhancing the photostability of the color converters and facilitating their integration with the  $\mu$ LEDs. These structures are less than 70  $\mu$ m in total thickness and are directly placed in contact with the polished sapphire substrate of 450-nm-emitting  $\mu$ LEDs. Blue-to-green, blue-to-orange, and blue-to-red conversion with respective forward optical power conversion efficiencies of 13%, 12%, and 5.5% are reported. In turn, free-space optical communications up to 1.4 Gb/s VLC is demonstrated. Results show that CQD-converted LEDs pave the way for practical digital lighting/displays with multi-Gb/s capability.

**Index Terms:** Visible light communications (VLCs), quantum dots, color converters.

## 1. Introduction

Colloidal quantum dots (CQDs) have emerged as an attractive luminescent nanomaterial for lighting and displays, in part because of their solution processability, narrow emission linewidth and broad absorption spectra. In this work, CQDs are combined with flexible glass and microsize GaN light-emitting diodes ( $\mu$ LEDs) to form optical sources for visible light communications (VLC). VLC is an emerging technology that uses white and/or colored light to combine illumination and display functionality with the transmission of data. VLC thereby transform LED bulbs and displays into emitters for new wireless communication networks in order to meet the data bandwidth requirements of future wireless applications and the Internet of Things [1]–[3]. The format of the CQD color converter that is presented here enables simple integration with LEDs, photostable color conversion and importantly addresses the problem of the modulation speed/wavelength coverage trade-off otherwise faced by the GaN LED technology.

GaN LEDs are enabling efficient solid-state lighting and displays. Moreover, these light sources have relatively high modulation speeds, making them attractive for added digital functionalities such as sending data optically in VLC, or Li-Fi, systems [4]. Multi-Gb/s free-space and fiber-based VLC using a blue-emitting LED and spectrally efficient modulation schemes was recently reported [5]. The latter demonstrations made use of  $\mu$ LEDs, which can withstand high current density leading to carrier-lifetime-limited modulation bandwidth in excess of 500 MHz [5]. These  $\mu$ LEDs are fabricated through microelectronic processes using industry standard LED wafers. Because of the existence of the so-called green-yellow gap, which is the spectral region where the efficiency of LEDs drops significantly [6], most LEDs for lighting and displays, i.e. with colors that span the visible spectrum, use color-converting materials. Blue-emitting LED chips optically excite yellow, green and/or red down-converting phosphors, eventually mixing the wavelengths to obtain light of the desired characteristics. This is currently the most efficient and cost-effective approach to generate yellow-green wavelengths and white light. However, conventional rare-earth phosphors have long luminescence lifetimes ( $\mu$ s to ms) severely limiting the performance of these LED sources for VLC; this is because the fluorescence lifetime of a material and the speed at which it can respond to modulated excitation light are intrinsically linked [7], [8]. White phosphor-converted LEDs have been demonstrated in VLC by filtering the phosphor-converted light at the receiver side [9], but this approach has limitations in terms of power penalty and signal to noise and is not compatible with applications where fully converted sources are needed (e.g. in displays).

CQDs form an alternative class of color converter [10], [11] with high photoluminescence quantum yield (PLQY) in the solid state and with optical properties that are tunable across the whole visible spectrum. CQDs have short radiative lifetimes, in the range of 10 to 50 ns [12], [13] for chalcogenide CQDs, as well as a narrower emission spectrum when compared to phosphors, making them more attractive for displays and VLC applications. Despite this, their true capability for VLC had not been demonstrated prior to this work. A challenge, common to all solution-processed light-emitting materials, is to find a format of color converter that is robust [14], [15] and practical for integration with LEDs. Here, we propose and demonstrate CQD color converters with enhanced photostability using flexible glass for both encapsulation and CQD interfacing with blue GaN  $\mu$ LEDs. Glass [16] and ultra-thin glass [17], [18] are known to be excellent encapsulating barriers for light-emitting organic materials and we postulated that ultra-thin (flexible) glass should perform similarly for CQDs.

In the following, Section 2 presents the design, fabrication and optical properties of the devices. Section 3 reports on the device dynamics and the VLC demonstration. Section 4 details the experimental methods and gives additional information on the fabrication and on the photostability of the color converters.

## 2. Design, Fabrication and Optical Properties

The hybrid LED consists of flexible-glass encapsulated CQD color converters in physical contact with the polished sapphire epitaxial substrate of a 450-nm-emitting  $\mu$ LED array (see Fig. 1). Each  $\mu$ LED pixel of the array is square and has a  $100\ \mu\text{m} \times 100\ \mu\text{m}$  emitting area. Alloyed-core

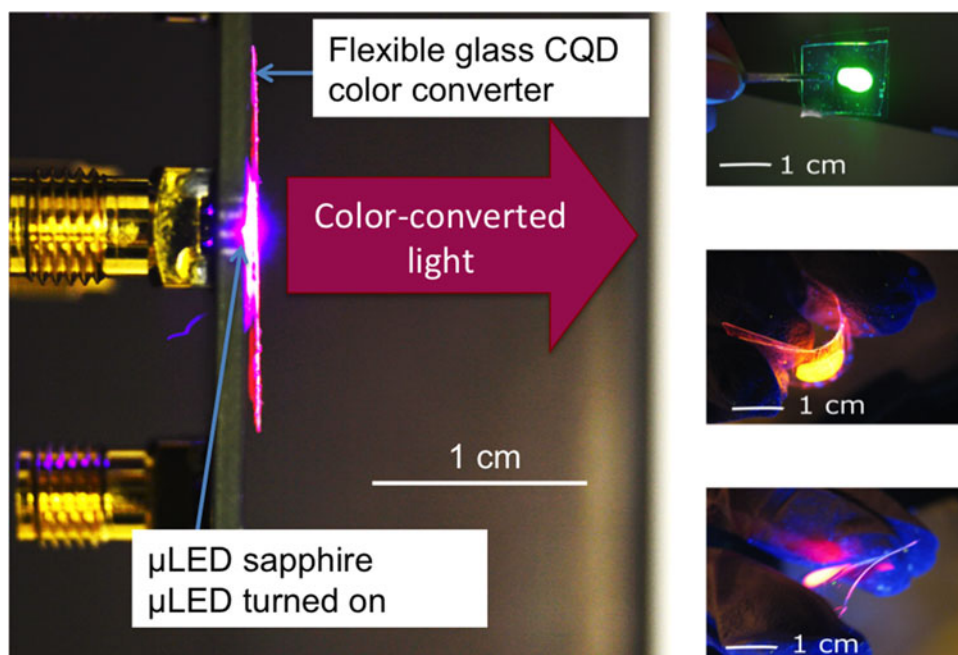


Fig. 1. Side-view of the device with CQD color converter pumped by the blue-emitting  $\mu$ LED with side-emitted converted (red) light visible in the flexible glass - the  $\mu$ LED array is mounted on a PCB with SMA connectors that can be seen on the left side; and (right) photographs of color converters, made (from top to bottom) with green, orange and red CQDs, respectively.

$\text{CdS}_x\text{Se}_{1-x}/\text{ZnS}$  CQDs emitting in the green (540 nm intrinsic wavelength), orange (575 nm) and red (630 nm) are used as the color converting material. These CQDs are 6-nm in nominal diameter and their emission wavelength is set by the alloy composition. CQDs are dissolved in chloroform at specific concentrations and then deposited on a 30- $\mu\text{m}$ -thick flexible glass membrane (AF32 thin glass from Schott) to form a CQD film. More details are given in Section 4. After drying the CQD film in air for a few minutes, another identical glass membrane is placed on top of the CQD film. The edges of the sample are sealed with a UV curable epoxy, NOA65 (Norland). Finally the sample is illuminated with UV light for a total exposure dose of 100  $\text{mJ}/\text{cm}^2$ . Flexible glass was chosen as it represent a good oxygen barrier and was previously used to encapsulate solution-based lasers [17]. Moreover, its flexibility facilitates the integration of the color converters with microLEDs. The  $\mu$ LED (peak wavelength of 450 nm) light absorption by the CQD film can be set by tailoring the concentration and deposition conditions of the initial CQD solution. Here, the converters that are presented and discussed absorb 97% or more of the blue light. The fabricated color converters under blue excitation can be seen in Fig. 1. Because the total thickness of the structure is below 70  $\mu\text{m}$ , it can be bended by mechanically flexing of the glass. The color-converters are then placed onto the polished sapphire substrate of a  $\mu$ LED array to yield the hybrid, color-converted source. Each  $\mu$ LED emits in the forward direction a maximum optical power of 8 mW for a 150 mA current. This blue light is absorbed and re-emitted as longer wavelength light by the CQD film. The  $\mu$ LED excitation spot diameter at the sapphire/thin-glass converter interface is 330  $\mu\text{m} \pm 20 \mu\text{m}$  and the associated pump power density is around 50  $\text{mW}/\text{cm}^2$  [16]. Details on the characteristics of the  $\mu$ LED are given in Section 4.

Spectra of the color-converted  $\mu$ LED are displayed in Fig. 2(a) for the three wavelengths of color converters (the spectral density response of the detector is calibrated and the intensity data is normalized to the maximum of the green emission). The peak emission wavelengths are found to be 572 nm, 606 nm and 650 nm for the green, orange and red devices, respectively. The color converter emission is red-shifted with respect to the intrinsic photoluminescence (PL) of the CQDs because of self-absorption of the color-converted photons in the closely packed CQD film. The

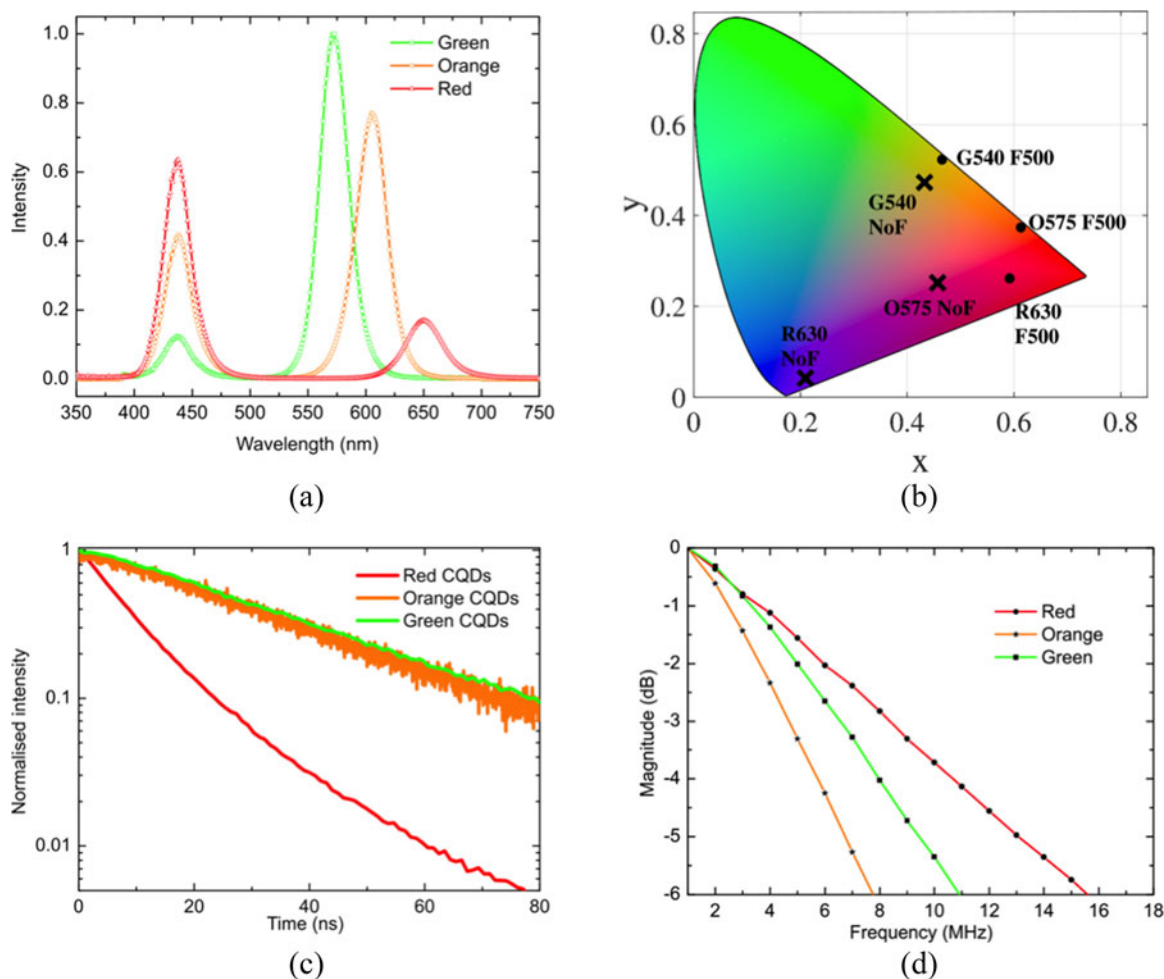


Fig. 2. (a) Electro-luminescence spectra of hybrid  $\mu$ LEDs, (b) CIE color diagram with the coordinates corresponding to the filtered and unfiltered hybrid  $\mu$ LEDs, (c) luminescence lifetime of the red, orange and green CQDs and (d) frequency response for these samples (filtered  $\mu$ LEDs).

unabsorbed  $\mu$ LED light peaking at 450 nm can also be seen in the spectra. The different colors obtained with these hybrid  $\mu$ LEDs with and without a long-pass filter (i.e. with and without the few percent of unabsorbed  $\mu$ LED light) are also represented in the CIE diagram of Fig. 2(b). The photostability of the flexible glass/CQD converters under constant blue LED excitation is found to be significantly enhanced compared to a non-encapsulated CQD film (see Section 4) with a  $\times 10$  to  $> \times 200$ -times improvement in operational lifetime compared to the equivalent non-encapsulated converter. Photodegradation of CQDs is attributed to photooxidation, which is mitigated in the flexible glass converters. Photodegradation starts in the samples once oxygen has permeated the epoxy sealing the edges of the flexible glass and reached the CQD films. This takes between ten to more than 250 hours in our converters and during that time color conversion is stable. Glass sintering to seal the edges of the flexible glass sheets would therefore be a way to further significantly extend the photostability of these CQD converters.

The PLQY of the equivalent CQD films is 62%, 54% and 18% for the green, orange and red CQDs, respectively. The variation of the PLQY according to the emission wavelength of the CQDs can be explained by the design of the material itself. The wavelength of the alloyed-core CdS<sub>x</sub>Se CQDs is tuned by varying the S/Se composition ratio. For longer wavelengths, the amount of sulphide is reduced, which increases the lattice mismatch with the ZnS shell and causes more stress. This can sometimes lead to defects that are detrimental to the PLQY [17]. The forward conversion

efficiency (the ratio of the power of the converted light, as measured in the forward direction by the experimental system, by the power of the bare  $\mu$ LED, see Section 4.3) for each wavelength of color converter is consistent with the PLQY. The green, orange and red color converters have respective forward conversion efficiency of 13%, 12% and 5.5%. The conversion efficiency and PLQY are consistent with the measured optical spectra. The forward power conversion efficiency values are lower than the PLQY because of the quantum defect and because light emitted in other directions, included light waveguided in the CQD film and the flexible glass, is not detected by the system. However, these values are higher than the 2% to 5% that could be expected if only considering light within the escape cone of the flexible glass/CQD film structure. This is due to photon recycling with some of the waveguided light being scattered out of the structure and some being reabsorbed by the CQDs and partially re-emitted in the forward direction. It should be possible to increase the forward conversion efficiency by (i) incorporating light extraction features in the film and/or the ultra-thin glass, and/or (ii) by adding a dichroic coating on the backside of the structure to reflect converted light in the forward direction.

The results of time resolved luminescence measurements on the samples are shown in Fig. 2(c). The light emitted by all 3 CQD color converters decays on a nanosecond timescale. The orange and green CQD films PL decays are monoexponential (over the studied range of 0–80 ns) with similar lifetimes of, respectively,  $33.5 \pm 0.5$  ns and  $34 \pm 0.5$  ns. The PL decay of the red CQDs is substantially faster with an average lifetime of  $13 \pm 4$  ns for a biexponential decay with rates  $\tau_1 = 8.2 \pm 0.1$  ns (weight  $A_1 = 86\%$ ) and  $\tau_2 = 23.5 \pm 1.2$  ns (weight  $A_2 = 14\%$ ). The shortest rate (8.2 ns) for the red CQDs is attributed to carrier trapping non-radiative recombinations [19], due to a higher level of defects. The longest component (23.5 ns) of the PL lifetime can be compared to those of the orange and green CQDs. The difference is explained by the degree of electron delocalization in the orange and green CQDs, which is caused by the lower electronic band offset between the core and shell regions (this offset diminishes as the S/Se ratio increases). Therefore, in the red CQDs the electron and hole wavefunctions overlap more strongly, leading to a shorter radiative lifetime. Overall, these PL lifetime values (between 13 ns and 35 ns) are at least two orders of magnitude shorter than for conventional phosphors.

### 3. Frequency Response and VLC

The frequency responses of the CQD color-converters are obtained by modulating the  $\mu$ LED with a frequency-swept signal and recording the amplitude of the color converted signal at the different frequencies. The results are plotted in Fig. 2(d). The  $-6$  dB values correspond to the optical bandwidth, i.e. the frequency at which the optical power is half the DC (direct current) value. Optical bandwidths of 8 MHz, 11 MHz and 16 MHz are found for, respectively, the orange, green and red CQDs for a DC bias of 3.8 V. The higher bandwidth of the red color converter was expected because of its shorter luminescence lifetime. The luminescence lifetime is directly related to the optical bandwidth by the following formula [1]:

$$B = \frac{\sqrt{3}}{2\pi\tau} \quad (1)$$

In (1),  $B$  is the optical bandwidth and  $\tau$  the fluorescence lifetime. Based on this formula and the measured average fluorescence lifetimes for each type of CQDs (see Fig. 2(c)), the respective calculated bandwidths are, 8.2 MHz, 8.3 MHz and 21 MHz, which are close to the values obtained from the frequency response measurements. Slight differences are to be expected as the frequency response measured is also dependent on the response of the underlying LED, although this dependency is small because the modulation bandwidth of the  $\mu$ LED is, except at low driving current, close to 10 times higher than that of the CQDs (see Section 4, Fig. 4).

Having established the optical properties of the  $\mu$ LED-integrated CQD color converters, free-space VLC demonstrations with the hybrid color-converted  $\mu$ LEDs are performed using orthogonal frequency division multiplexing (OFDM) as the data encoding method. OFDM is a multi-carrier scheme that enables the efficient utilization of the bandwidth of an optical source,

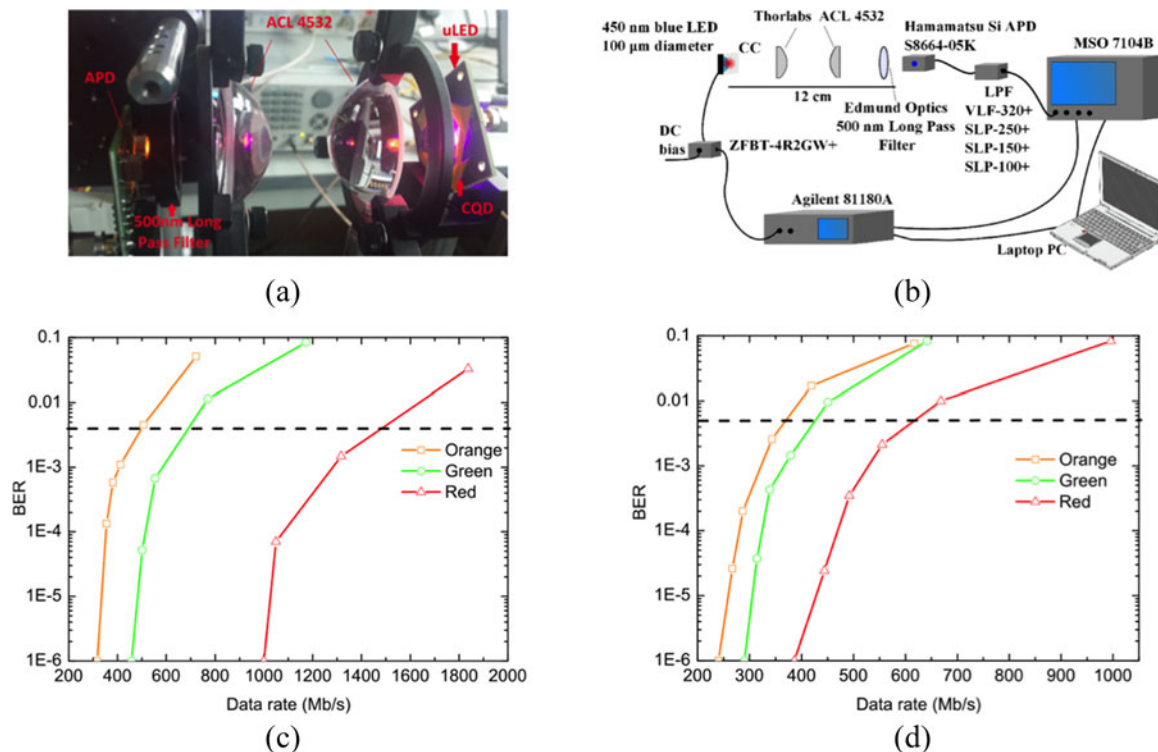


Fig. 3. (a) Photograph of the VLC set-up with the hybrid  $\mu$ LED on the right and the APD on the left, (b) schematic of the VLC set up, (c) data rates against the BER for the hybrid  $\mu$ LEDs with no filter and (d) for the hybrid  $\mu$ LEDs with filter (e.g. color converted light only).

utilizing frequencies past the optical bandwidth. Data streams are sent onto the orthogonal frequency subcarriers distributed over the bandwidth of the optical channel. Here, each sub-carrier is modulated using multi-level quadrature amplitude modulation (M-QAM), the sub-carrier spacing being equal to a multiple of the symbol duration. The constellation sizes and the associated power of M-QAM symbols are adaptively allocated to each subcarrier based on the estimated signal to noise ratio at that exact frequency band. The symbols are then multiplexed into a discrete time domain output using inverse fast Fourier transformation (IFFT). The OFDM signal is clipped and DC-biased (DCO-OFDM) based on the electrical-optical characteristic of the  $\mu$ LED. The generation of OFDM waveform and all the associated signal processing is performed using MATLAB. The OFDM signal is fed into the LED using an arbitrary waveform generator Agilent 81180 A. A DC-bias is added to the bipolar OFDM signal using a Bias-T ZFBT-4R2GW.

The  $\mu$ LED device with integrated color converter placed on the VLC link demonstrator can be seen Fig. 3(a). A schematic of the VLC experiment is shown in Fig. 3(b). The underlying blue  $\mu$ LED is modulated using the OFDM signal and the resulting intensity modulated signal is color converted to longer wavelengths by the CQDs. The light is collimated at the source side using an aspheric condenser lens ACL 4532 at the  $\mu$ LED front and then focused at the detection side using a similar lens. An avalanche photodiode (APD) Hamamatsu-S8664-05, active area of 0.19 mm<sup>2</sup>, is used as the receiver. The received signal is captured by an oscilloscope MSO7104B, and then processed offline with MATLAB. It is then fast Fourier transformed (FFT) and post-equalization is performed on the recovered M-QAM symbols before the demodulation process. The overall distance between the  $\mu$ LED and the APD is 12 cm. Two channels are used to drive two  $\mu$ LED pixels (from the same array) in parallel in a so-called ganging mode (i.e. the signals driving the two  $\mu$ LEDs signals are identical), in order to increase the optical power at the receiver. An optical long-pass filter, to block the unabsorbed blue light, is optionally added in front of the APD when the data signal carried only by the color converted light is studied. With no filter, the full hybrid device emission is collected.

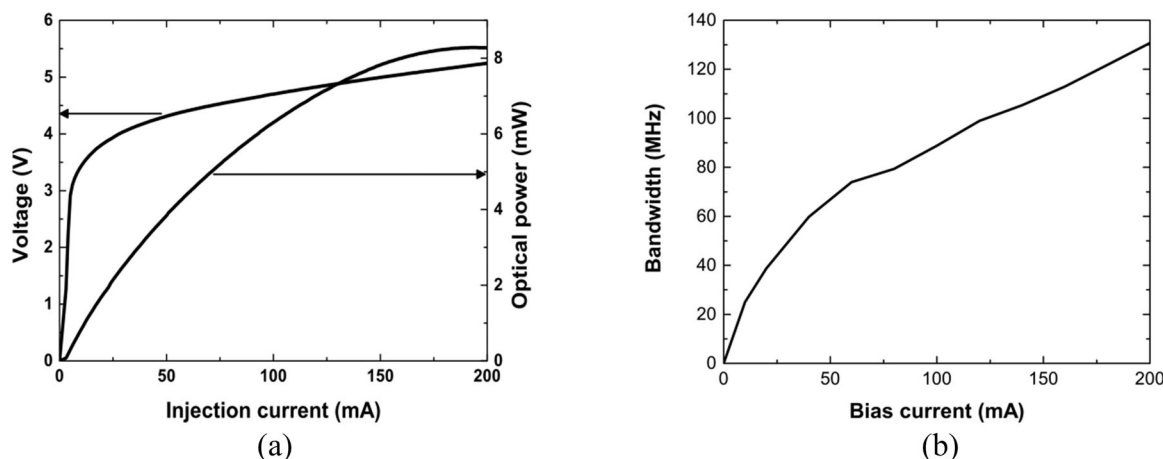


Fig. 4. Characteristics of the  $\mu$ LED: (a) voltage and forward collected optical power versus injection current; (b) optical bandwidth versus driving current.

The different colors obtained from only the color-converters (using an optical filter) and from the hybrid  $\mu$ LEDs (without optical filters) are shown in Fig. 2(b). The hybrid  $\mu$ LEDs without a filter are represented by the first letter of the color (G, O and R) followed by the emission wavelength (540 nm, 575 nm and 630 nm) and NoF (for 'no optical filter'). The colors obtained from the color-converted light alone are represented by the first letter of the color and the wavelength followed by F500 (for 'long pass filter with 500 nm cut-off wavelength'). We note that the performance versus the transmission distance is not studied and that no optimization of the light collection is carried out. However, the VLC distance could be scaled up through a number of approaches, for example: by using several  $\mu$ LEDs working in tandem to increase the overall emitted optical power; by increasing the light extraction from the color-converter, e.g. by texturing the flexible glass; by adding a dichroic coating on one of the surfaces of the flexible glass in order to re-direct the backward emitted color converted signal; by optimising the collection optics.

Fig. 3(c) and (d) plot the bit error ratio (BER) measured as a function of the data rates. The data rate values quoted next correspond to a maximum BER of  $3.8 \times 10^{-3}$  [20]. This is the typical value in optical wireless experiments considering that forward error corrections can be implemented. The red CQDs show the highest data rate of 617 Mb/s for R630 F500, and 1473 Mb/s for R630 NoF, partly because of their shorter fluorescence lifetime. For the orange CQDs, a data rate of 370 Mb/s is obtained for O575 F500 and 496 Mb/s for O575 NoF. Concerning the green CQDs, 428 Mb/s is achieved for G540 F500 and 692 Mb/s for G540 NoF. Note that the higher data rates obtained when no filter is used is caused by the few percent of unabsorbed blue light. These data rates values are, to our knowledge, the highest data rates transmitted via CQDs and represents an up to 40-time improvement compared to previous data rates obtained from chalcogenide CQDs converters [10].

## 4. Experimental Methods and Additional Information

### 4.1 Color Converters

Details of different test samples studied to optimize the fabrication process are summarized Table 1. CQDs were drop-coated or spin-coated for 60 s in order to form the color converting films between the flexible glass sheets. For each color, the recipe giving the highest converted power was selected to demonstrate hybrid  $\mu$ LEDs in OFDM VLC. Overall, it can be seen that the efficiencies of the green and orange CQDs are similar while it is lower for the red CQDs. This is consistent with the PLQY of these materials. It can also be noted that at high absorption, above 99%, the efficiency of the color converters drops and this for all 3 colors. Such an effect is caused by the re-absorption of the color-converted photons, which is enhanced in a highly absorbing film. Green1, Orange2 and Red2

TABLE 1

CQD Color-Converting Samples; Concentrations of Starting CQD Solutions, Film Deposition Method (rpm for Rotations Per Minute), Absorption, Forward Emission Conversion Efficiency and Bandwidth

Samples	Concentration (mg/mL)	Deposition	Absorption (%)	Efficiency (%)	Bandwidth (MHz)
Red1	10	drop coated	81.6 $\pm$ 0.4	5.6 $\pm$ 0.2	20.4
Red2	20	drop coated	97.1 $\pm$ 0.6	5.0 $\pm$ 0.1	18.8
Red3	70	spin 500 rpm	97.3 $\pm$ 0.2	2.0 $\pm$ 0.1	15.6
Orange1	70	drop coated	97.5 $\pm$ 0.4	11.3 $\pm$ 0.3	10.4
Orange2	70	drop coated	97.8 $\pm$ 0.2	12.0 $\pm$ 0.2	11.6
Orange3	70	spin 300 rpm	99.9 $\pm$ 0.1	9.3 $\pm$ 0.2	7.7
Green1	70	drop coated	97.4 $\pm$ 0.4	13.3 $\pm$ 0.4	11
Green2	70	drop coated	98.7 $\pm$ 0.5	10.8 $\pm$ 0.2	6.8
Green3	70	drop coated	99.6 $\pm$ 0.4	5.3 $\pm$ 0.2	8.3

were the recipes selected for the OFDM experiments, because of their higher converted power (adequate trade-off absorption and conversion efficiency). The error given on the values in Table 1 is the standard deviation of the measurement for each sample (the samples are measured several times, removing and re-setting the sample in the apparatus each time). It can be noted in Fig. 2(a) that the LED absorption by the green sample is higher than the orange sample, while based on Table 1 they are expected to be similar. This discrepancy can be explained by the repeatability of the fabrication process, which can be influenced by factor such as temperature and air humidity. The error on the absorption due to fabrication repeatability is estimated at  $\pm$  1%.

#### 4.2 $\mu$ LED

The  $\mu$ LEDs are fabricated using a commercial p-i-n GaN structure as described in [21]. The voltage versus current and forward-collected optical power versus current for a typical single LED pixel by itself (with no CQD color converter) is shown in Fig. 4(a). The current-dependent frequency response of such a LED is plotted in Fig. 4(b). The  $-3$ dB optical modulation bandwidth reaches up to 120 MHz at 180 mA.

#### 4.3 Forward Conversion Efficiency and Optical Spectra

The light emitted in the forward direction by the color converter is collected and imaged by two aspheric lenses having each a focal length of 32 mm and a high numerical aperture ( $NA = 0.612$ ). The light collected is measured through a long-pass filter for the determination of the converted light power and through a short-pass filter for the determination of the unabsorbed LED light. The absorbed blue light is obtained by taking the difference of the optical power of the LED measured by the set-up (when there is no color-converting film) minus the unabsorbed blue light. The forward conversion efficiency of the color converter is the measured optical power of the converted light divided by this absorbed blue light.

Optical spectra are recorded with Labsphere spectral irradiance receiver head (E1000) with a maximum spectral resolution of 1 nm.

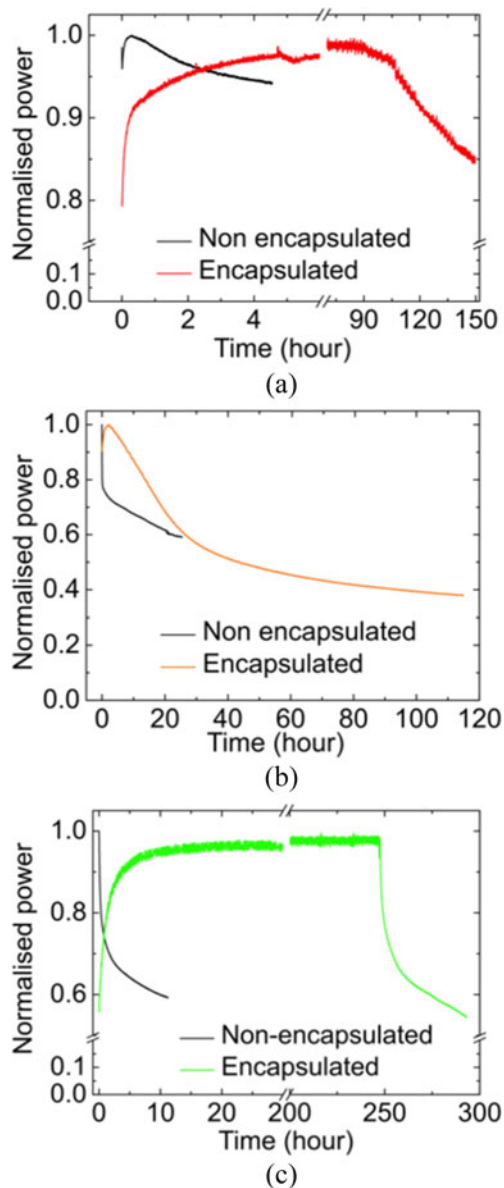


Fig. 5. Photostability of the encapsulated and non-encapsulated (a) red, (b) orange and (c) green CQD color converters.

#### 4.4 PL Quantum Yield and PL Lifetime

To perform these measurements, solutions of each type of CQDs are spin-coated on a quartz substrate. Each sample is then placed in a 10 cm diameter integrating sphere and optically excited with a helium-cadmium laser (wavelength of 475 nm). The PLQY is then measured using a calibrated silicon photodiode (Graseby-UDT 221) using the procedure described in [22].

PL lifetimes are measured using the time correlated single-photon counting technique. The CQD samples are excited by a pulsed LED (Picoquant, model PLS 370), emitting at 393 nm and with 10 pJ/pulse at a pulse repetition rate of 10 kHz. The light emitted by the sample is detected by a microchannel plate photomultiplier tube (Hamamatsu, model RU-3809U-50). The instrument response function is 250 ps. The decay kinetics are then extracted by fitting the normalized intensity data as a function of time with an exponential or a bi-exponential decay function.

#### 4.5 Bandwidth

For bandwidth measurements the color converter is placed directly on top of the  $\mu$ LED, as can be seen Fig. 1. The  $\mu$ LED is driven by an AC (alternating current) signal combined with a DC bias of 3.8 V. The amplitude of the AC frequency-swept modulated signal ( $V_{pp}$ ) is 650 mV and the sinusoidal frequency is varied from 100 kHz to 300 MHz. The emission is collected and collimated by optics, and further filtered to block any residual blue LED light. Finally, a third lens is used to focus the light into an Omega-2 APD (3 mm<sup>2</sup> detector area APD). The amplitude of the detected signal, proportional to the square of the optical power, is plotted as a function of the modulation frequency. The optical bandwidth corresponds to the frequency at which the optical power is half that of the low frequency value.

#### 4.6 Photostability

Non-encapsulated CQDs color-converters (without the second glass membrane protecting the thin film of CQDs) were made in order to assess the beneficial effect of the converter format on photostability. The emission intensity level over time is measured, for both encapsulated and non-encapsulated samples, under constant excitation for a pump power density of 50 mW/cm<sup>2</sup>. Results are plotted in Fig. 5(a), (b) and (c). It can be seen that the intensity initially increases with time of exposure for most samples, in particular for all encapsulated samples. This effect of photo-annealing happens within the first few hours of exposure for the encapsulated samples and is known to happen for CQDs [23]. After this photoannealing stage, the emission intensities of the red and the green encapsulated color converters are stable for around 4.5 and 10 days, respectively. The intensity then slowly decreases (by 20% and 40% over 60 hours respectively for the red and green samples), a degradation that can be explained by photooxidation of the CQDs [23]. The intensity decreases on a much shorter timescale for all the non-encapsulated devices. In fact it is almost immediate when compared to the encapsulated samples (it starts decreasing within the first hour) and the annealing stage is limited and in some cases absent. This faster degradation is consistent with a photooxidation process as air, and hence oxygen, is in direct contact with the CQDs in non-encapsulated samples. The flexible glass protects the CQDs and prevents their luminescence from degrading via this process. However, oxygen can still permeate the epoxy sealing the edges over time, reaching the active area after tens of hours. As opposed to the green and red samples, the encapsulated orange CQD sample has a shorter annealing phase followed by the start of the intensity decay after only a couple of hours. This seems to indicate an issue with encapsulation for this particular sample. However, the measurement was repeated on another orange sample with similar results. Further investigations are on going to understand this. Even though, the encapsulated format also benefits the photostability of the orange CQDs. Overall, the format of the flexible glass CQD color converter enhances the photostability of the CQDs. A fabrication process done in a nitrogen environment should further extend the photostability of the samples even further. Indeed, other types of photonics device made with CQDs have shown extended lifetime (above 30 000 hours) [24], [25].

### 5. Conclusion

In conclusion, we have demonstrated high-speed VLC using  $\mu$ LEDs color converted by CQDs. We reported an ultra-thin-glass encapsulated color-converting structure for enhanced photostability and interfacing with  $\mu$ LEDs. Blue to red, orange and green forward optical power conversion efficiencies of, respectively, 5.5%, 12% and 13% were obtained. The optical modulation bandwidths of the CQDs converters is up to 16 MHz. Free-space data transmissions up to 1.4 Gb/s were achieved with CQD hybrid LEDs driven using OFDM. Such performance was enabled by the luminescence properties of the CQDs and by the format of the color converter. In addition, the wavelength versatility of CQDs permits such performance across the visible spectrum while their narrow emission linewidth is also attractive for wavelength division multiplexing, whereby data is sent in parallel using different colors.

## Acknowledgment

N. Laurand thanks M. Leitao for the photograph of the device shown in Fig. 1. Supporting data is available at DOI: 10.15129/d4d7d1d3-c220-4965-81b4-6a0de3824717.

## References

- [1] H. Haas, L. Yin, Y. Wang, and C. Chen, "What is LiFi?" *J. Lightw. Technol.*, vol. 34, no. 6, pp. 1533–1544, Mar. 2016.
- [2] H. Haas, "A light-connected world," *Phys. World*, vol. 29, no. 8, pp. 30–34, 2016.
- [3] D. C. O'Brien, L. Zeng, H. Le-Minh, G. Faulkner, J. W. Walewski, and S. Randel, "Visible light communications: Challenges and possibilities," in *Proc. IEEE 19th Int. Symp. Pers. Indoor Mob. Radio Commun.*, vol. 19, no. 1, pp. 1–5, 2008.
- [4] A. Jovicic, J. Li, and T. Richardson, "Visible light communication: opportunities, challenges and the path to market," *IEEE Commun. Mag.*, vol. 51, no. 12, pp. 26–32, Dec. 2013.
- [5] X. Li *et al.*, "Wireless visible light communications employing feed-forward pre-equalization and PAM-4 modulation," *J. Lightw. Technol.*, vol. 34, no. 8, pp. 2049–2055, Apr. 2016.
- [6] M. Auf der Maur, A. Pecchia, G. Penazzi, W. Rodrigues, and A. Di Carlo, "Efficiency drop in green InGaN/GaN light emitting diodes: The role of random alloy fluctuations," *Phys. Rev. Lett.*, vol. 116, no. 2, pp. 027401–027405, 2016.
- [7] T. Komine and M. Nakagawa, "Fundamental analysis for visible-light communication system using LED lights," *IEEE Trans. Consum. Electron.*, vol. 50, no. 1, pp. 100–107, Feb. 2004.
- [8] C. H. Yeh, Y. L. Liu, and C. W. Chow, "Real-time white-light phosphor-LED visible light communication (VLC) with compact size," *Opt. Exp.*, vol. 21, no. 22, pp. 26192–26197, 2013.
- [9] A. M. Khalid, G. Cossu, R. Corsini, P. Choudhury, and E. Ciaramella, "1-Gb/s transmission over a phosphorescent white LED by using rate-adaptive discrete multitone modulation," *IEEE Photon. J.*, vol. 4, no. 5, pp. 1465–1473, Oct. 2012.
- [10] N. Laurand *et al.*, "Colloidal quantum dot nanocomposites for visible wavelength conversion of modulated optical signals," *Opt. Mater. Exp.*, vol. 2, no. 3, pp. 250–260, 2012.
- [11] S. Nizamoglu, G. Zengin, and H. V. Demir, "Color-converting combinations of nanocrystal emitters for warm-white light generation with high color rendering index," *Appl. Phys. Lett.*, vol. 92, no. 3, pp. 113110–113113, 2008.
- [12] V. Klimov, "Nanocrystal quantum dots," *Los Alamos Sci.*, vol. 28, no. 203, pp. 214–220, 2003.
- [13] T. H. Kim *et al.*, "Full-colour quantum dot displays fabricated by transfer printing," *Nature Photon.*, vol. 5, no. 3, pp. 176–182, 2011.
- [14] E. P. Jang, W. S. Song, K. H. Lee, and H. Yang, "Preparation of a photo-degradation-resistant quantum dot polymer composite plate for use in the fabrication of a high-stability white-light-emitting diode," *Nanotechnology*, vol. 24, no. 4, pp. 1–9, 2013.
- [15] H. Peng, L. Zhang, C. Soeller, and J. Travas-Sejdic, "Preparation of water-soluble CdTe/CdS core/shell quantum dots with enhanced photostability," *J. Lumin.*, vol. 127, no. 2, pp. 721–726, 2007.
- [16] S. Richardson, O. P. M. Gaudin, G. A. Turnbull, and I. D. W. Samuel, "Improved operational lifetime of semiconducting polymer lasers by encapsulation," *Appl. Phys. Lett.*, vol. 91, no. 26, pp. 261104–261107, 2007.
- [17] C. Foucher, B. Guilhabert, J. Herrnsdorf, N. Laurand, and M. D. Dawson, "Diode-pumped, mechanically-flexible polymer DFB laser encapsulated by glass membranes," *Opt. Exp.*, vol. 22, no. 20, pp. 24160–24168, 2014.
- [18] C. Foucher, B. Guilhabert, N. Laurand, and M. D. Dawson, "Wavelength-tunable colloidal quantum dot laser on ultra-thin flexible glass," *Appl. Phys. Lett.*, vol. 104, no. 14, pp. 141108–141112, 2014.
- [19] G. A. Beane, K. Gong, and D. F. Kelley, "Auger and carrier trapping dynamics in core/shell quantum dots having sharp and alloyed interfaces," *ACS Nano*, vol. 10, pp. 3755–3765, 2016.
- [20] ITU-T Recommendation G.975.1, Appendix I.9, 2004.
- [21] Z. Gong *et al.*, "Efficient flip-chip InGaN micro-pixelated light-emitting diode arrays: promising candidates for micro-displays and colour conversion," *J. Appl. Phys.*, vol. 107, no. 1, pp. 013103–013109, 2010.
- [22] N. C. Greenham *et al.*, "Measurement of absolute photoluminescence quantum efficiencies in conjugated polymers?" *Chem. Phys. Lett.*, vol. 241, no. 1, pp. 89–86, 1995.
- [23] K. Pechstedt, T. Whittle, J. Baumberg, and T. Melvin, "Photoluminescence of colloidal CdSe/ZnS quantum dots: The critical effect of water molecules," *J. Phys. Chem. C*, vol. 114, no. 28, pp. 12069–12077, 2010.
- [24] J. Chen, V. Hardev, J. Hartlove, J. Hoffer, and E. Lee, "A high-efficiency wide-color-gamut solid-state backlight system for LCDs using quantum dot enhancement film," *SID Symp. Dig. Tech. Papers*, vol. 43, no. 1, pp. 895–896, 2012.
- [25] H. Chen, J. He, and S. T. Wu, "Recent advances on quantum-dot-enhanced liquid-crystal displays," *IEEE J. Sel. Topics Quantum Electron.*, vol. 23, no. 5, Sep./Oct. 2017, Art. no. 1900611.